Catena xxx (2008) xxx–xxx

Contents lists available at ScienceDirect

Catena

journal homepage: www.elsevier.com/locate/catena

A simultaneous model for ultrasonic aggregate stability assessment

A. Fristensky [a], M.E. Grismer [b,*]

[a] Hydrologic Sciences, UC Davis, Davis CA 95616, United States
[b] Departments of LAWR and Biological and Agricultural Engineering, 1 Shields Ave UC Davis, Davis CA 95616, United States

ARTICLE INFO

Article history:
Received 10 September 2007
Received in revised form 31 March 2008
Accepted 10 April 2008
Available online xxxx

Keywords:
Comminution
Particle-size distributions
Ultrasonic analyses
Modeling

ABSTRACT

Aggregate stability is a difficult to quantify, complex soil property. Ultrasonic processing of soil–water suspensions enables quantifiable and readily reproducible assessment of the level of mechanical energy applied to soil aggregates. Here, we present a method of investigating the stability and comminution of soil aggregates by simultaneously modeling the redistribution of particles throughout any arbitrarily-selected set of soil particle-size intervals as ultrasonic energy is applied to a soil–water suspension. Following model development, we demonstrate its application to 5 particle-size subgroups (0.04–2000 μm) of a Dystroxerept subject to 12 levels of ultrasonic energy between 0 and 5800 J g^{-1} (750 mL^{-1}). Laser granulometry was used for particle-size distribution (PSD) analysis, providing precise, non-disruptive measurements of changes in the volume of PSD subgroups in both the microaggregate (<250 μm; 3 subgroups) and macroaggregate (>250 μm; 2 subgroups) fractions throughout ultrasonic treatment. Two groups of aggregates were detected exhibiting significantly ($p<0.05$) different ultrasonic stability: a group composed exclusively of macroaggregates ranging 250–2000 μm in size, and a finer, relatively stable group ranging 20–1000 μm. The PSD of particles liberated from two aggregate groups significantly ($p<0.05$) differed: the coarser, less-stable group liberated 13% clay (0.04–2 μm), 53% fine silt (2–20 μm), and 34% coarse silt and sand (20–250 μm); while the finer, more-stable group liberated 26% clay and 74% fine silt. The ultrasonic energy required to disrupt 25%, 50%, and 75% of all aggregates within a given PSD interval significantly ($p<0.05$) differed between all selected intervals, showing a trend of declining stability with increasing particle-size. Both the flexibility of the proposed model and the extension of ultrasonic stability assessment to simultaneous analysis of both microaggregate and macroaggregate subgroups can facilitate broader application of ultrasonic methods to soil processes related research.

1. Introduction

Aggregate stability is a highly complex parameter influencing a wide range of soil properties, including carbon stabilization, soil porosity, aeration, compactibility, crustability, water retention, hydraulic conductivity, and resistance to detachment and transport by wind, raindrop impact, and overland flow. A variety of techniques have been developed for measuring this parameter (Amezketa, 1999). Among these, ultrasonic processing of soil–water suspensions has attracted considerable investigation (North, 1976; North, 1979; Imeson and Vis, 1984; Fuller and Goh, 1992; Levy et al., 1993; Raine and So, 1993; Raine and So, 1994; Tippkotter, 1994; Field and Minasny, 1999; Field et al., 2006). In contrast to most conventional methods, the ability to quantify the level of mechanical energy applied to soil (North, 1976; Raine and So, 1993) enables the results of ultrasonic stability tests to be quantified and compared in a continuous index of treatment intensity. Also, ultrasonic processing allows considerable control and flexibility over both the power and total energy of application. This allows aggregate comminution to be observed and modeled over a desired range of applied energy, offering the advantage of representing aggregate stability as a rate of resistance to fragmentation, rather than as the fraction of aggregates remaining following a treatment of often arbitrary intensity or duration. Furthermore, simultaneously modeling the comminution of aggregates in more than one range of aggregate particle-sizes (e.g. <2 μm, 2–20 μm, 20–2000 μm) can offer insight into aggregate comminution dynamics and aggregate hierarchy (Field and Minasny, 1999; Field et al., 2006).

This study presents a model of the redistribution of particles throughout a soil particle-size distribution (PSD) as aggregates comminute under ultrasonic agitation. The proposed model enables investigation of the stability, component PSD, and hierarchy of soil aggregates by simultaneously modeling total mass changes in any selected set of PSD partitions (i.e., $[x_1, x_2]$, $[x_2, x_3]$,..., $[x_{n-1}, x_n]$) as ultrasonic energy is applied to a soil–water suspension. The goal of this development is to enhance the flexibility and resolution of ultrasonic aggregate stability assessment. The model is also intended to be universally applicable. That is, it does not presume studied aggregates to possess a particular hierarchical structure, or to comminute according to a particular pathway under ultrasonic agitation (Field and Minasny, 1999; Field et al., 2006). The model also allows for the possibility that aggregate fragmentation may

* Corresponding author. Tel.: +1 530 752 3243 (off.).
E-mail addresses: afristensky@ucdavis.edu (A. Fristensky), megrismer@ucdavis.edu (M.E. Grismer).

0341-8162/$ – see front matter © 2008 Published by Elsevier B.V.
doi:10.1016/j.catena.2008.04.013

directly release both aggregates and primary particles. Similar to previous ultrasonic studies that used exponential functions to model aggregate breakdown (Fuller and Goh, 1992; Levy et al., 1993; Raine and So, 1993; Raine and So, 1994; Tippkotter, 1994; Raine and So, 1997), and following Field and Minasny (1999) and Field et al. (2006) who modeled aggregate comminution according to an analogue of a first-order consecutive reaction, we assume that the breakdown of a quantity of aggregates (of equal stability) under ultrasonic agitation follows first-order decay. However, the proposed approach differs from previous studies in that aggregates are classified according to their observed resistivity to ultrasonic agitation, rather than according to particle-size. This can facilitate detection and modeling of distinct aggregate groups of similar stability that possess (along with their liberated fragments) PSDs that overlap the selected set PSD partitions. This approach also accounts for the possibility that groups of aggregates with distinctly different stability (as well as their liberated fragments) may possess PSDs which overlap, or fall within the same selected PSD partition(s).

In addition to proposing an ultrasonic aggregate comminution model, we consider use of ultrasonic methods for targeted analysis of aggregate particle-size subgroups in both the macroaggregate (>250 μm, e.g. 1000–2000 μm) and microaggregate (<250 μm) fractions. While most ultrasonic aggregate stability studies have used ultrasound to disrupt both macroaggregates and microaggregates, the PSD fractions subject to analysis have invariably fallen partly or entirely within the microaggregate fraction (e.g. 20–2000 μm). However, aggregate stability varies significantly with particle-size and hierarchical order (Edwards and Bremner, 1967; Braunack et al., 1979; Tisdall and Oades, 1982; Dexter, 1988; Oades and Waters, 1991), and aggregates may liberate a range of particle-sizes. High PSD resolution across both the microaggregate (Levy et al., 1993; Field et al., 2006) and macroaggregate fractions is therefore desirable for characterizing aggregate stability and comminution. However, the classical methods of PSD determination – the pipette and hydrometer methods (Gee and Bauder, 1986) – have limited capacity for resolving PSD intervals, and are highly sensitive to laboratory technique and operator error (Beuselinck et al., 1998; Eshel et al., 2004). Moreover, the technique employs sieving to separate larger, rapidly settling particles from clay and silt particles. Sieving imparts an unquantifiable mechanical stress to the soil, and thus separating macroaggregate subgroups would partly negate one of the principle benefits of using ultrasound to disrupt aggregates (i.e., quantifiable energy application). To circumvent these limitations, we employ the laser-light diffraction technique for PSD analysis (Eshel et al., 2004). The laser diffraction technique can be used to perform precise, virtually non-disruptive analysis of soil–water suspensions, and enables calculation of an essentially continuous soil PSD. Morra et al. (1991) and Levy et al. (1993) employed the laser-light diffraction technique to measure changes in the PSD of the silt-sized and <105 μm fractions, respectively, across different levels of applied ultrasonic energy. Here, we expand the analysis to include discrete microaggregate and macroaggregate subgroups between 0.04 and 2000 μm. Considering that aggregate stability assessment is usually conducted in the context of soil erosion research, targeted investigation of macroaggregate fractions – important to soil hydraulic conductivity and vulnerable to raindrop impact and tilling – can offer a useful enhancement to ultrasonic aggregate stability assessment.

Following a detailed presentation of the proposed modeling approach below, we illustrate an application of the proposed model to a Dystroxerept subject to various levels of ultrasonic agitation. The model is applied to experimental data representing the volume of particles within each of 5 PSD intervals – [0.04–2 μm], [2–20 μm], [20–250 μm], [250–1000 μm], and [1000–2000 μm] – throughout ultrasonic treatment. These particular intervals were selected to generally correspond with previous aggregate stability studies, as well as the aggregate hierarchy model proposed by Tisdall and Oades (1982), and the functional classification of soil particle-sizes presented in Oades (1984).

2. Methods and materials

2.1. Model development

As shockwaves generated from ultrasound-induced cavitation propagate throughout a soil–water suspension, the bonds cohering discrete soil particles into aggregates may become disrupted, leading to aggregate fragmentation. If the liberated particles consist of yet smaller aggregates, these may continue to break down under added stress. This process of aggregate disruption continues until the state of complete soil fragmentation and dispersion into primary particles (clay, silt, sand) is reached, or until the point at which the power applied is inadequate to overcome the strength of the remaining aggregate bonds. If a hierarchy exists, an inverse relationship between aggregate order and strength may be explained by the ‘porosity exclusion principle’ (Dexter, 1988) which holds that superordinate aggregates have greater porosity than subordinate aggregates due to pore spaces existing between the smaller, denser constituent particles. These pores are planes of weakness that increase aggregate susceptibility to fragmentation when mechanical stress is applied (Braunack et al., 1979; Utomo and Dexter, 1981). Aggregate stability also depends upon the different types of bonding mechanisms operating across different size scales. For example, ramifying plant roots or mycorrhizal hyphae may enmesh soil particles together into macroaggregates (>250 μm); plant debris and polysaccharides excreted by bacteria, fungi and roots may be important in the formation and binding of microaggregates (<250 μm); and clay flocculation along with polyvalent cation bridging of clay with recalcitrant, decomposed organic matter are important binding agents at the <20 μm scale (Tisdall and Oades, 1979; Oades, 1984; Oades and Water, 1991).

Considering the observed link between aggregate strength, size, and prevailing bonding mechanisms, it seems reasonable to expect that a group of aggregates characterized by a common set of binding agents may exhibit a similar resistance to disruption by ultrasonic agitation. Building upon this concept, Fig. 1 illustrates a framework for describing aggregate comminution by organizing aggregates into groups, or “cohorts”, according to their observed resistivity to ultrasonic agitation. Note that the y-axis in Fig. 1 is positive in both directions from the origin to allow for a more convenient display of information.

The x-axis represents particle diameter (μm). The illustrated curves represent PSDs as the differential mass of particles of size x relative to the total mass of particles in that group. Curves shown below the y-axis origin (1, 2, 3) represent groups of aggregates (“cohorts”) defined by a characteristic rate of breakdown. Curves above the origin (*I*, *II*, *III*) represent the distribution of discrete particles (aggregates and primary particles) liberated from aggregate cohorts. The dashed arrows between the curves denote the relationship between a given cohort and its liberated particles. For example, 1 → *I* represents the breakdown of cohort 1 aggregates to yield the distribution, *II*, of liberated discrete particles. Aggregates of cohort 2 include all aggregates falling under the definition of cohort 2 prior to disturbance, whether these exist discretely, or are initially assimilated into aggregates of higher hierarchical order(s). Conversely, the distribution *II* is defined as the size distribution of all discrete particles, including aggregates, liberated from cohort 2 aggregates upon fragmentation. More precisely, *II* is the distribution of particles that would occur if cohort 2 was isolated, and thereafter only cohort 2 aggregates (but not their liberated aggregates) were permitted to break down. Note, no hierarchical ordering is implied by the lettering of cohorts 1, 2, 3, etc. Particles liberated from a given aggregate are permitted to include discrete subordinate aggregates belonging to any number of cohorts.

It is also important to note that this model of aggregate breakdown assumes that all aggregates – whether initially assimilated into larger aggregates or existing discretely – are continuously agitated and subject to fragmentation throughout the applied ultrasonic treatment. This assumption would not account for the possibility that

Please cite this article as: Fristensky, A., Grismer, M.E., A simultaneous model for ultrasonic aggregate stability assessment, Catena (2008), doi:10.1016/j.catena.2008.04.013

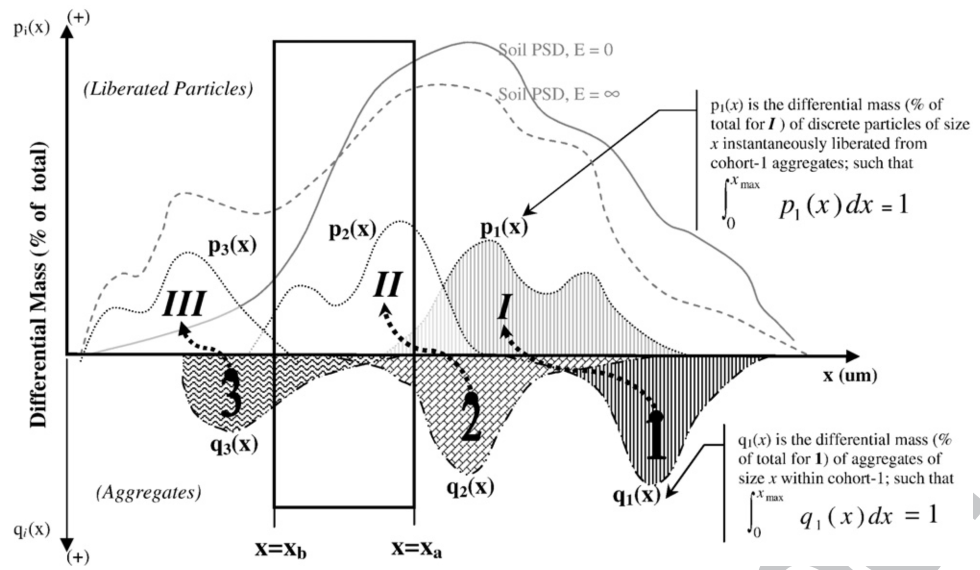

Fig. 1. Conceptual framework for describing aggregate comminution, illustrating arbitrary distributions of aggregates and their fragments.

microaggregates bound in the interior of a larger aggregate may be shielded from agitation until they are exposed or liberated. In other words, this approach does not incorporate the concept of a threshold level of ultrasonic energy needed to initiate the comminution of aggregates of a particular size or stability.

The functions $q_i(x)$ (noted in Fig. 1) represent the differential mass of aggregates of size x relative to the total mass of aggregates composing the ith cohort (i=1, 2,..., n). That is, $q_2(x)$ describes the size distribution of cohort 2 aggregates, such that $\int_0^{x_{\max}} q_2(x)dx = 1$, where $x_{\max}$ is the maximum particle-size diameter of the soil subject to analysis. Similarly, the functions $p_i(x)$ are the differential mass of particles of size x liberated from the ith cohort relative to the total mass of particles liberated from the ith cohort; i.e. $p_2(x)$ describes the distribution *II*, such that $\int_0^{x_{\max}} p_2(x)dx = 1$. Overlap is possible between the domains of two or more different $q_i(x)$, reflecting the concept that the size ranges at which a given set of aggregate bonding agents operate may extend into range at which different agents also operate.

With these definitions and notation, we present a stepwise construction of an equation that models aggregate comminution by measuring changes in the total mass of an arbitrarily-selected interval $[x_b, x_a]$ of a soil PSD as ultrasonic energy (E) is applied. This interval is outlined in Fig. 1, and illustrated in greater detail in Fig. 2. Note that the curves representing cohort 2 in Fig. 2 are conceptually identical as those of Fig. 1, except that they denote the absolute (rather than relative) differential mass of aggregates and liberated particles of a given size x. Essentially, the problem to be solved is a mass-balance equation of inputs and loss of material from the range $[x_b, x_a]$ as aggregates break down. For clarity, first only changes in $[x_b, x_a]$ occurring as a consequence of the breakdown of cohort 2 aggregates will be modeled — these results will then be extended to encompass all aggregates.

Suggested by Fig. 2, the total mass of particles of size $x_b<x<x_a$ liberated from cohort 2 aggregates can be represented as

$$b_2\int_{x_b}^{x_a} p_2(x)dx = b_2\left[\int_{x_b}^{x_a} q_2(x)\theta(x)dx + \lambda\int_{x_a}^{x_{\max}} q_2(x)(1-\phi(x))dx\right] \tag{1}$$

where b_2 is the total mass of cohort 2 aggregates; $\theta(x)$ is the mass proportion of particles of size $x_b<x<x_a$ liberated from aggregates of size $x\in[x_b, x_a]$; $\phi(x)$ is the mass proportion of particles of size $x_a<x<x_{\max}$ liberated from aggregates of size $x\in[x_a, x_{\max}]$; and λ is the mass proportion of all liberated particles of size $x<x_a$ that are of size $x>x_b$, obtained from aggregates of size $x>x_a$. Dashed arrows representing $\theta(x)$, $\phi(x)$, and λ are shown in Fig. 2.

However, it is clear from inspection of Fig. 2 that the first of the two terms on the right-hand side of Eq. (1) has no net impact on the total mass of the interval $[x_b, x_a]$, because the mass $b_2q_2(x)\theta(x)$ is neither contributed to, or lost from, this interval. This observation is important to consider when reporting calculated total mass of aggregated particles, as it indicates that the total observed loss of material within a PSD interval due to aggregate comminution is always less than or equal to the actual initial amount of material composing aggregates within that interval. However, the magnitude of errors due to this effect is expected to decline as the width of selected PSD intervals is reduced.

To preclude misleading reporting of total aggregated material, the system of notation developed above will be modified to reflect only measurable changes in the total mass of $[x_b, x_a]$ due to aggregates comminution. First, the particle-size intervals $[x_a, x_{\max}]$, $[x_b, x_a]$, and $[0, x_b]$ will hereafter be called "tiers" A, B, and C, respectively, as illustrated in Fig. 2. The term $q_{2A}(x)\equiv(1-\phi(x))q_2$ $x\in[x_a, x_{\max}]$ is introduced to be analogous to $q_2(x)$ but reflecting the distribution of mass of particles of size $x<x_a$ assimilated into tier A aggregates. Similarly, $q_{2B}(x)\equiv(1-\theta(x))q_2$, $x\in[x_b, x_a]$ is the distribution of mass of particles of size $x<x_b$ assimilated in tier B aggregates. Also, the term $p_{2A}(x), x\in[0, x_a]$ is introduced to be analogous to $p_2(x)$ but reflecting the size distribution of particles of size $x<x_a$ liberated from tier A aggregates; and similarly for $p_{2B}(x)$ with respect to particles of size $x<x_b$ liberated from tier B aggregates. Hypothetical curves representing the $b_2(q_{2A}(x))$, $b_2(q_{2B}(x))$, and $b_{2A}(p_{2A}(x))$ are shown in Fig. 2.

With these definitions, the right-hand side of Eq. (1) can be rewritten to reflect only the mass of liberated particles of size $x_b<x<x_a$ that have a measurable impact (contribution) on the total mass of tier B:

$$\begin{aligned} & b_2\left[0+\lambda\int_{x_a}^{x_{\max}} q_2(x)(1-\phi(x))dx\right] \\ & \quad = b_2\lambda\int_{x_a}^{x_{\max}} q_{2A}(x)dx = b_{2A}\int_{x_b}^{x_a} p_{2A}(x)dx, \\ & \quad \text{where } b_{2A}\equiv b_2\int_{x_a}^{x_{\max}} q_{2A}(x)dx. \end{aligned} \tag{2}$$

Similarly, a term can be obtained representing the total measurable loss of mass from tier B due to comminution of tier B aggregates:

$$b_2\int_{x_b}^{x_a} q_2(x)(1-\theta(x))dx = b_2\int_{x_b}^{x_a} q_{2B}(x)dx \equiv b_{2B}. \tag{3}$$

Having obtained terms representing the total input and loss of mass from tier B due to aggregate comminution, the instantaneous mass of tier B at a given level of applied ultrasonic energy, E, can be obtained by incorporating terms describing the rate at which these

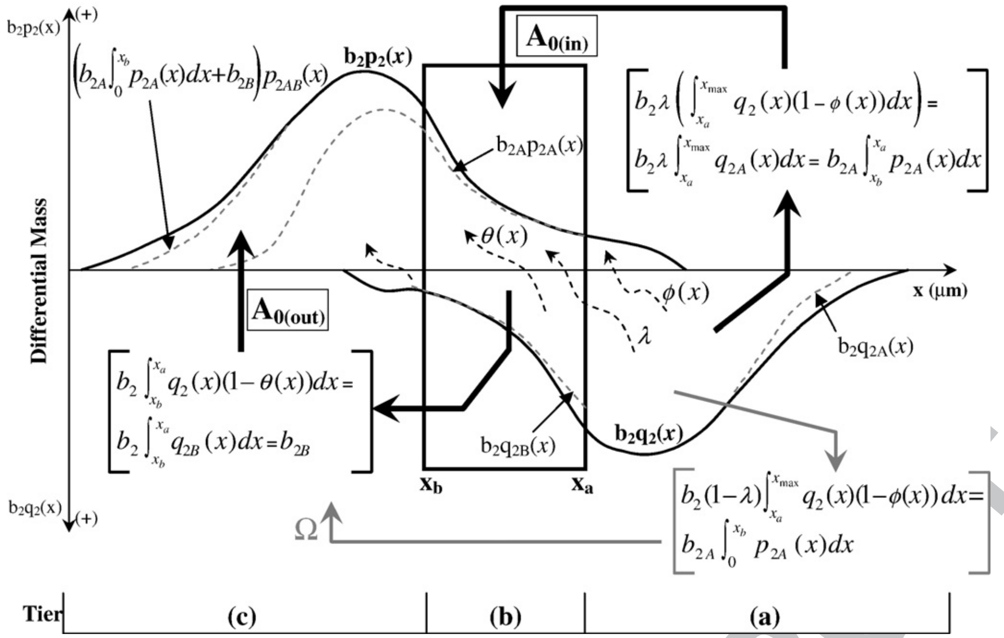

Fig. 2. Illustration of the redistribution of particles throughout arbitrary PSD partitions due to ultrasonic agitation. Shown in bold arrows are the measurable total gain ($A_{0(in)}$) and loss ($A_{0(out)}$) of mass of the PSD interval [x_b, x_a] (tier B) due to aggregate comminution.

aggregates break down under ultrasonic agitation. Similar to Field and Minasny (1999) and Field et al. (2006), we assume that for a quantity of aggregates (of equal stability) the disintegration of aggregated particles A into fragments F, or $A \rightarrow F$, with increasing E follows first-order decay. However, we are interested in the rate of contribution of F to tiers B and C. Considering the reaction $A \rightarrow F$, the rate of change of the total quantity of fragments is equal but opposite to the rate of change in the total quantity of aggregated particles. Integrating, an exponential expression describing the total quantity of fragments F liberated from aggregates at any level of E is obtained:

$$F(E) = F_0 + A_0\left(1 - e^{-aE}\right). \tag{4}$$

Eq. (4) is identical in form to the model employed by Raine and So (1993). In this context, however, the parameter $F_0 = F(0) = 0$ indicates that no particles have been liberated prior to the application of energy.

Letting $A_{0(in)}$ and $A_{0(out)}$ be defined as the total mass of aggregate fragments contributed to, and lost from, tier B during aggregate comminution (respectively), the cumulative mass of fragments contributed to ($F(E)_{in}$) and lost from ($F(E)_{out}$) tier B at a given level E can be described: Q2

$$F(E)_{(in)} = A_{0(in)}\left(1 - e^{-a_2E}\right) = \left(b_{2A}\int_{x_b}^{x_a} p_{2A}(x)dx\right)\left(1 - e^{-a_2E}\right) \tag{5}$$

$$F(E)_{(out)} = A_{0(out)}\left(1 - e^{-a_2E}\right) = b_{2B}\left(1 - e^{-a_2E}\right) \tag{6}$$

where a_2 is the rate constant associated with cohort 2 aggregates. The quantities $A_{0(in)}$ and $A_{0(out)}$ are illustrated in Fig. 2. The total mass of particles within tier B, or $D_{[B]}(E,x)$, at a given level E can thus be expressed:

$$\begin{aligned} D_{[B]}(E,x) &= F(E)_{IN} - F(E)_{OUT} + D_{0B} \\ &= \left[b_{2A}\int_{x_b}^{x_a} p_{2A}(x)dx - b_{2B}\right]\left(1 - e^{-a_2E}\right) + D_{0B} \end{aligned} \tag{7}$$

where D_{0B} is the initial mass of tier B. However, as will become clear during the following development of a simultaneous system of equations representing the mass of multiple tiers, a more convenient parameterization of Eq. (7) is Q3

$$\begin{aligned} D_{[B]}(E,x) &= \left[b_{2A}\left(\int_0^{x_a} p_{2A}(x)dx - \int_0^{x_b} p_{2A}(x)dx\right) - b_{2B}\right]\left(1 - e^{-a_2E}\right) + D_{0B} \\ &= \left[b_{2A}\left(1 - \int_0^{x_b} p_{2A}(x)dx\right) - b_{2B}\right]\left(1 - e^{-a_2E}\right) + D_{0B} \end{aligned} \tag{8}$$

This form provides a term that accounts for the particles liberated from tier A aggregates that fall within tier C but not tier B, as illustrated by the quantity Ω in Fig. 2.

Finally, as the effect of the breakdown of aggregate cohorts upon the mass of tier B is additive, a model of the form (8) describing the effect of all cohorts on the mass of tier B can be obtained by repeating the same procedure above for each cohort, and summing each result. In summation notation, this model is:

$$D_{[B]}(E,x) = D_{0B} + \sum_{i=1}^{n}\left[b_{iA}\left(1 - \int_0^{x_b} p_{iA}(x)dx\right) - b_{iB}\right]\left(1 - e^{-a_iE}\right). \tag{9}$$

A simultaneous system of equations based on Eq. (9) is now developed in order to simultaneously model changes in the total mass of any arbitrary set of PSD tiers (e.g. tiers A, B, C, D, etc.) due to comminution of aggregates under ultrasonic agitation. The basic problem is identical to that of Eq. (9) – i.e. a mass-balance of particles contributed to and lost from a given tier – but with the added complexity of tracking particles across multiple tiers. In fact, Eq. (11) already implicitly expresses behavior of three adjacent tiers – tiers A, B, and C – although only changes in tier B are explicitly stated. The mass of these three tiers at a given level of E is represented by the following system of equations: Q4 Q5

$$\begin{aligned} D_{[A]}(E,x) &= \delta_{0A} + \sum_{i=1}^{n} b_{iA}e^{-a_iE} \\ D_{[B]}(E,x) &= D_{0B} + \sum_{i=1}^{n}\left[b_{iA}\left(1 - \int_0^{x_b} p_{iA}(x)dx\right) - b_{iB}\right]\left(1 - e^{-a_iE}\right) \\ D_{[C]}(E,x) &= D_{0C} + \sum_{i=1}^{n}\left[b_{iA}\left(\int_0^{x_b} p_{iA}(x)dx\right) + b_{iB}\right]\left(1 - e^{-a_iE}\right) \end{aligned} \tag{10}$$

where δ_{0A} is the total mass of primary particles within tier A. This system expresses the loss of material from tier A (i.e. b_{iA}) occurring at

Please cite this article as: Fristensky, A., Grismer, M.E., A simultaneous model for ultrasonic aggregate stability assessment, Catena (2008), doi:10.1016/j.catena.2008.04.013

Table 1
Summary of site information and soil characteristics (Soil Survey Staff, 2007)

Series	Location (WGS 84)	Elevation (m)	Aspect	Slope (deg)	Taxonomy	Surface texture
Tallac	39 11′ 33.6″N, 120 13′ 02.4″W	2040	NW	20	Loamy-skeletal, mixed, superactive, frigid humic Dystroxerepts	Gravelly coarse sandy loam

rate a_i; a contribution of some proportion of this material to tier B, offset by the breakdown of tier B aggregates (b_{iB}); and an increase in the mass of tier C due to contributions from tiers A and B (i.e., the quantities Ω_i and $A_0A_{0i(\mathrm{out})}$ illustrated for the single-cohort scenario in Fig. 2). Note that the parameters b_{iA} and corresponding a_i are represented in tiers A, B, and C; and that the parameters b_{iB} and corresponding a_i are represented in B and C. In the context of nonlinear regression, the parameters to be estimated include the a_i, b_{ij} for the jth tier, integrals of the $p_{iA}(x)$, δ_{0A} and the D_{0j}.

To extend this development to a 4-tier system, consider the case in which tier C has a nonzero lower bound, x_c. Let tier D represent the fraction $[0, x_c]$. The change in volume of tiers C and D with applied energy would then be:

$$\begin{aligned} D_{[C]}(E,x) &= D_{0C} + \sum_{i=1}^{n}\left[\left(b_{iA}\left(\int_0^{x_b} p_{iA}(x)\mathrm{d}x\right) + b_{iB}\right)\right.\\ &\quad \left.\times\left(1-\int_0^{x_c} p_{iAB}(x)\mathrm{d}x\right) - b_{iC}\right](1-e^{-a_iE}) \\ D_{[D]}(E,x) &= D_{0D} + \sum_{i=1}^{n}\left[\left(b_{iA}\left(\int_0^{x_b} p_{iA}(x)\mathrm{d}x\right)+b_{iB}\right)\left(\int_0^{x_c} p_{iAB}(x)\mathrm{d}x\right)\right.\\ &\quad \left. + b_{iC}\right](1-e^{-a_iE}) \text{ where } p_{iAB}(x) = \frac{b_{iA}p_{iA}(x)+b_{iB}p_{iB}(x)}{b_{iA}\left(\int_0^{x_b} p_{iA}(x)\mathrm{d}x\right)+b_{iB}}. \end{aligned} \tag{11}$$

Due to the fact that the mass $b_{iA}\int_0^{x_b} p_{iA}(x)\mathrm{d}x$ and b_{iB} are distributed to the $<x_b$ fraction at the same rate (a_i) for the ith cohort, it is not possible to distinguish between $p_{iA}(x)$ and $p_{iB}(x)$ by measuring total mass changes in the $<x_b$ fraction. Hence, the terms $p_{iAB}(x)$, $x\in[0, x_b]$ are introduced to represent the combined distribution of these particles. In other words, $\int_0^{x_c} p_{iAB}(x)\mathrm{d}x$ represents the proportion of ith cohort liberated particles of size $x<x_b$ that are also smaller than x_c. Fig. 2 illustrates a curve representing the $p_{2AB}(x)$, indicated in the upper left-hand corner. Note that if the ith cohort is represented in tier B but not tier A, then $p_{iAB}(x)=p_{iB}(x)$, because $p_{iA}(x)=0$ for all x.

Expansion of the system to any number of tiers can be accomplished according to the same rational employed to obtain the 4-tier system above. For instance, analogous to the $p_{iAB}(x)$ for the 4-tier system, a 5-tier system must include the terms $p_{iABC}(x)$ must be introduced, to represent the combined distribution of particles $<x_c$ liberated from all ith cohort aggregates $>x_c$. The example analysis below employs a 5-tier system.

As this development illustrates, the model rapidly increases in complexity with each additional tier; and hence the number of tiers that can be practicably modeled is limited. Also, an unavoidable limitation of the model is that only net changes of mass within each tier can be detected, such that if particles are being contributed and lost from a given tier at the same rate (i.e. associated with the same cohort), the latter mass cannot be detected if it is smaller than the mass being contributed. If this "replacement" is occurring to a significant degree, the effect would be (1) smaller estimates of cohort mass; and (2) calculation of a finer distribution of liberated particles, and a coarser distribution of aggregate sizes, than the actual distributions of the given cohort (Fristensky, 2007).

2.2. Site

The soil investigated in this study was obtained in the Lake Tahoe Basin, California, U.S.A., from a forested slope located within the Resort at Squaw Creek complex in the South Fork Squaw Creek Watershed. The sample site is a research plot monitored by Integrated Environmental Restoration Services (IERS, Tahoe City, CA), as part of ongoing erosion abatement research. Local vegetation included white fir (*Abies concolor*), and pinemat manzanita (*Arctostaphylos nevadensis*), along with winter-green (*Pyrola picta*) and lousewort (*Pedicularis semibarbata*) (Integrated Environmental Restoration Services (IERS), 2007). A summary of soil site information and soil characteristics is presented in Table 1 (Soil Survey Staff, 2007).

Soil sampling was conducted in late August, 2006. Average soil moisture at time of sampling was measured by time-domain reflectometry (TDR) at approximately 10 cm depth. Three samples of approximately 500 g were obtained from the surface soil within a 400 ft^2 area to an approximate depth of 8–10 cm (excluding litter layer). The three soil samples allowed to air-dry, then gently dry-sieved to 2 mm, homogenized, and sealed at room temperature until analysis. The oven-dry (24 h at 105 °C) weight of the soil was determined to calculate the hygroscopic moisture content under laboratory conditions. Soil organic matter (Walkley–Black method) and soil pH was determined by the University of California Agricultural and Natural Resources lab. Table 2 reports the selected physical and chemical properties of the prepared soil.

2.3. Ultrasonic processing

Ultrasonic processing of soil samples was based closely upon the method and experimental investigations presented in Raine and So (1993, 1994). Ultrasonic processing was conducted using a Vibra-Cell® VCX-130, operating at 20 kHz with a maximum power output of 130-Watts, and using a 113 mm length, 6 mm diameter titanium-alloy probe. Subsamples of 4 g oven-dry equivalent weight each were processed in 45 mL centrifuge tubes (1.5 cm radius) in 31 mL of deionized (DI) water. Samples were rapidly immersed in DI water 30–60 min before processing. The ultrasonic probe was inserted into the soil suspension to a depth of 1.43 cm, with the probe centerline 0.6 cm from the container wall. During ultrasonification, subsamples were insulated with a 0.25 cm-thick polyurethane foam sheath tightly set within a polystyrene block with holes for the ultrasonic probe and temperature probe.

Ultrasonification of soil suspensions was conducted at constant amplitude for 12 different time periods between 0 and 1650 s (Table 3) in order to obtain a measure of the soil disruption over a wide range of applied energies. Three repetitions were performed for each period of applied energy. Processor amplitude was held constant at 65%, which was qualitatively determined to be the minimum level able to produce enough mixing to maintain circulation of the largest sand-sized particles. This amplitude applied 14.2±0.2 W (SE) of ultrasonic energy to the soil–water suspension, measured calorimetrically (Raine and So, 1993). Suspension temperature was maintained within the range of 20–35 °C by cooling suspensions to 20 °C in an ice bath after each 150-second period of applied energy (Raine and So, 1994).

Suspension temperature was measured during ultrasonic processing with a 24.5 cm, 0.318 cm diameter bendable 3-pin RTD integral-handle temperature probe, and a Digi-Sense® (Cole-Parmer Instrument Co, Vernon Hills, IL) ThermologR™ digital RTD thermometer.

Table 2
Selected properties of prepared sample

% Clay[a] (0.04–2 μm)	% Silt[a] (2–63 μm)	% Sand[a] (63–2000 μm)	% Soil moisture at time of sampling (TDR)	Total organic matter (%, Walkley–Black)	pH
11.6	67.6	20.8	5	15.2	5.5

[a] Reported PSD data reflects the soil state following ultrasonic treatment at the highest level of applied energy. No chemical dispersing agents were used.

Table 3
Sample PSD at different levels of treatment time (t) or energy (E)

PSD interval (μm)		Average volume (% of total soil) of PSD interval (±SD)				
t (s)	E (J g^{-1} (J mL^{-1}))	1000–2000	250–1000	20–250	2–20	0.04–2
0	0 (0)	9.9 (±1.3)	29.3 (±0.4)	48.2 (±0.6)	10.5 (±0.5)	2.1 (±0.1)
30	108 (14)	6.8 (±1.0)	22.1 (±1.0)	51.3 (±1.0)	16.4 (±0.6)	3.4 (±0.2)
60	215 (28)	3.9 (±1.0)	17.8 (±0.5)	53.3 (±0.2)	20.5 (±0.6)	4.4 (±0.2)
90	321 (41)	3.1 (±1.9)	15.5 (±1.0)	53.6 (±2.3)	22.8 (±0.5)	5.1 (±0.2)
150	532 (69)	1.1 (±0.4)	13.7 (±0.6)	53.0 (±1.4)	26.2 (±0.4)	6.1 (±0.2)
210	746 (96)	0.2 (±0.2)	12.1 (±1.2)	52.9 (±0.3)	28.2 (±1.1)	6.7 (±0.3)
330	1170 (151)	0.3 (±0.3)	11.8 (±2.6)	50.7 (±1.0)	29.9 (±2.6)	7.3 (±0.6)
450	1593 (206)	0.2 (±0.2)	10.5 (±1.4)	49.2 (±1.0)	32.0 (±1.3)	8.2 (±0.3)
690	2444 (315)	0.01 (±0.01)	8.4 (±1.4)	47.2 (±0.4)	35.2 (±1.4)	9.2 (±0.3)
930	3292 (425)	0.001 (±0.001)	6.2 (±0.1)	44.3 (±0.4)	38.9 (±0.1)	10.6 (±0.2)
1290	4565 (589)	0.0 (±0.0)	4.4 (±2.6)	44.0 (±1.5)	40.4 (±1.0)	11.2 (±0.4)
1650	5839 (753)	0.0 (±0.0)	4.9 (±2.3)	41.9 (±1.8)	41.6 (±0.6)	11.6 (±0.2)

The RTD probe was bent to approximately 40°, 13.97 cm from the probe tip (to allow access to the suspension during processing), and inserted to a depth of 6.19 cm at 1.2 cm radial distance from the ultrasonic probe centerline. Temperature was recorded at 11-second intervals during ultrasonification. The cooling characteristic curve of the system (probes, suspension, centrifuge tube, insulation material) was determined by heating a soil suspension to 40 °C, recording temperature at 1010-second intervals until the suspension reached room temperature, and fitting the data with a 6th-order polynomial regression function (using JMP statistical software, version 6, SAS Institute, Inc., 1989–2005). Heat capacity of the container (i.e. centrifuge tube, insulation material, probes) was 30.3±0.5 J °C^{-1} (SD)C^{-1}, estimated according to method of mixtures as presented in Roscoe et al. (2000).

Error propagation and uncertainty of all derived statistics were calculated according to Arras (1998).

2.4. Particle-size analysis

Particle-size analysis of processed soil suspensions was performed using a Beckman-Coulter LS-230 laser-light diffraction particle-size analyzer. Particle-size analysis of sonicated samples was completed within approximately 4–7 h of ultrasonic treatment. Samples were poured into the detection chamber pool, and diluted to the optimal device levels. Information obtained from the LS-230 PSD analysis included the volume (percent of total) of the soil particle-size fractions: <1000 μm, <250 μm, <20 μm, and <2 μm. From these data, the percent volume of the discrete particle-size ranges [1000–2000 μm], [250–1000 μm], [20–250 μm], [2–20 μm], and [0.04–2 μm] was calculated. These particle-size fractions are labeled as tiers A through E, respectively.

2.5. Nonlinear regression analysis

For the example analysis, the model system of equations was expanded to 5 PSD tiers – [1000–2000 μm], [250–1000 μm], [20–250 μm], [2–20 μm], and [0.45–2 μm] – with a maximum of 2 unique terms representing distinct aggregate cohorts included per tier. Nonlinear regression analysis of ultrasonic processing data for each tier was performed using JMP statistical software (JMP, version 6, SAS Institute, Inc., 1989–2005), using the JMP "Analytic NR' NR" iterative solving method. To minimize error propagation, regression analysis was performed simultaneously for all selected PSD tiers. This was achieved using JMP by organizing the model system of equations into a single stepwise function, and assigning each tier a unique range of energy values (Fristensky, 2007).

To obtain a regression model consisting of the fewest number of parameters (i.e. the simplest model) needed to adequately explain the data, variables selection procedures (both statistical and heuristic) were conducted. Heuristically, regression model selection proceeded according to the same basic concept guiding model development; namely, aggregate comminution proceeds from larger particles to smaller. Accordingly, variable selection began with the parameters representing cohorts within the coarsest tier, which were allowed to explain as much variation as possible throughout all finer tiers. Additional terms representing cohorts in finer tiers were then added to the model, competing with parameters previously entered into the model. F-tests were employed throughout this process to determine whether the reduction in the model error sum of squares (SSE) attained by inclusion of additional parameters was statistically significant when considering the associated loss of model degrees of freedom (Kutner et al., 2005). If the model successfully converged to the specified criterion, JMP was used to obtain confidence limits (CLs) for all parameters. If CLs bounded zero at the 95% level, the associated term was excluded from the analysis, and the (reduced) model was re-evaluated. If two modeled cohorts were found to possess reaction rate constants that did not significantly differ at the 95% level, they were considered to represent the same cohort. Also, in accordance with aggregate hierarchy theory and the porosity exclusion principle (Dexter, 1988), it was expected (although not strictly assumed) that larger aggregates would exhibit larger reaction rate constants compared to smaller aggregates. This overall model selection approach described above was not quite sufficient to obtain an appropriate model. It was clear at certain stages that the "best" fit either did not make physical sense (e.g. negative asymptote), or did not exhibit the expected form (e.g. a straight line fit due to outliers or large variance, where a curvilinear distribution was observed). Visual inspection of a graphical plot of the model throughout the variable selection process was very useful in identifying potential outliers as well as inappropriate parameter terms or values.

Once an appropriate model was selected, JMP was used to obtain the following statistics:

(a) parameter estimates, and associated confidence limits (CLs);
(b) SSE and mean square error (MSE) for both the whole model and for all individual tiers; and
(c) the variance–covariance matrix of all model parameters.

As a note, estimated CLs provided by JMP for nonlinear regression may not be symmetric about the expected value (SAS Institute, Inc., 2005). Q7

Functions of the estimated model parameter values were evaluated to derive the following secondary statistics:

(a) volume of (measurable) aggregated particles within each cohort and each tier;
(b) total volume of liberated particles from all tiers; and
(c) the volume of liberated particles contributed from each cohort to each tier.

The standard error of all secondary statistics were estimated according to Arras (1998), with associated CLs calculated according to Kragten (1994).

Please cite this article as: Fristensky, A., Grismer, M.E., A simultaneous model for ultrasonic aggregate stability assessment, Catena (2008), doi:10.1016/j.catena.2008.04.013

2.6. Model comparisons

Results of the proposed model were compared with the results of alternative models: a single exponential approach (or decay) function (see Eq. (4), where F_0 is the initial PSD tier volume, and A_0 is the total volume of particles liberated from the PSD tier); and the ALDC (Field and Minasny, 1999). These alternative models were fitted to experimental data using the nonlinear regression platform of JMP statistical software. Confidence intervals for all estimated parameters were obtained as described above. The alternative models considered for comparison are "nested" within the proposed ("full") model. Therefore, the relative appropriateness of the models can be compared using the *F*-test to determine whether the reduction in the model SSE attained by the inclusion of additional parameters is statistically significant when considering the associated loss of degrees of freedom (Kutner et al., 2005, p. 72–73). In other words, if the "reduced" model is assumed to be the correct model (H_0), the *F*-test ascertains the probability that the smaller SSE of the "full" model is due to random variation in the data. If this probability is very low (e.g. $p < 0.05$), the full model is taken as statistically more appropriate than the reduced model (H_a).

The simple exponential approach (or decay) function was fitted to data representing the <2 μm, 2–20 μm, <20 μm, and 250–1000 μm particle-size fractions. The ALDC (Field and Minasny, 1999) model was applied to the experimental dataset by simultaneous nonlinear regression analysis of the >250 μm and <20 μm fractions. Parameter estimates were obtained for k_1, k_2, and A_0 according to the equations provided in Field and Minasny (1999). The model

$$\mathrm{ALDC} = -A_0[\exp(-k_1 E) - \exp(-k_2 E)] + C_2 \tag{12}$$

was then applied to the 20–250 μm fraction, by inserting the parameter estimates obtained earlier. In this analysis, C_2 was allowed to vary freely to account for the initial volume.

2.7. E_{25}, E_{50}, and E_{75}

Similar to Fuller and Goh (1992), comparisons of aggregate stability in this study are based on the level of energy required to reach benchmark states of aggregate breakdown. The indices selected for comparison are E_{25}, E_{50}, and E_{75}, the energy (J g^{-1}) required to liberate 25%, 50% and 75%, respectively, of the aggregated particles within a given PSD tier. Three states of soil disruption were selected in order to highlight relative soil behavior across a wide range of applied energy. However, inverse predictions of the energy required to reach a particular state of breakdown are not trivial to calculate when more than one rate constant characterizes aggregate breakdown within a PSD tier of interest. For example, consider the following 2-cohort model for a given PSD tier, describing strictly the volume of aggregated particles ($b_1 + b_2$):

$$A = b_1 e^{-a_1 E} + b_2 e^{-a_{21} E}. \tag{13}$$

The energy term *E* cannot be isolated through algebraic manipulation:

$$E = \frac{-\ln\left(\frac{A - b_1 e^{-a_1 E}}{b_2}\right)}{a_2}. \tag{14}$$

In order to obtain a prediction of *E* at a given level of *A*, numerical approximation methods must be invoked. Here, Mathematica (version 5.1.0.0, Champaign, IL, 1988–2004) was utilized for numerical solving, using the *FindRoot* function. Confidence limits for E_{25}, E_{50} and E_{75} were estimated according to the method of Alvord and Rossio (1993), again using Mathematica for numerical solving.

3. Results and discussion

3.1. Particle-size analysis

Laser-light diffraction particle-size analysis of treated samples provided precise results for all selected PSD tiers and across all levels of applied ultrasonic energy (Table 3). Fig. 3 graphically presents the PSD data for each tier as a function of applied energy. The results indicate both precision in the PSD measurement method and high reproducibility of the ultrasonic tests. Notably, steady changes in the volume of macroaggregate (>250 μm) PSD tiers were observed with increasing energy application, indicating that the laser-light technique is able to resolve the progressive breakdown of macroaggregate subgroups under ultrasonification. Because the laser-light diffraction method requires no separate, disruptive treatment for large particle-sizes (e.g. wet sieving), these results demonstrate this method to be

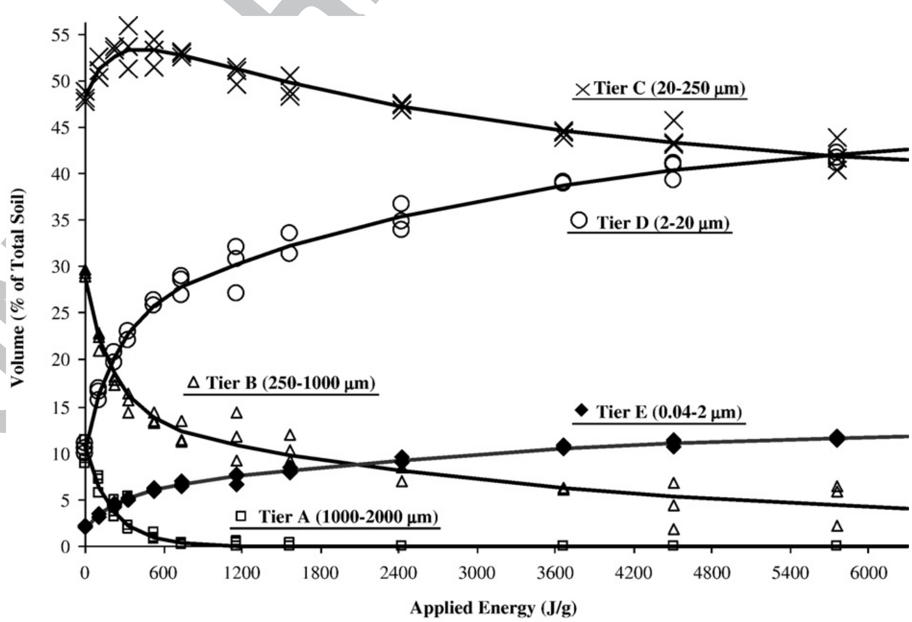

Fig. 3. Simultaneous nonlinear regression modeling of ultrasonic processing data for all selected PSD tiers.

aptly suited for targeted ultrasonic stability assessment of both microaggregates (<250 μm) and macroaggregates (250–2000 μm).

3.2. Aggregate stability and comminution modeling

The aggregate fragmentation model developed above was successfully fit by nonlinear regression to the particle-size data obtained from the ultrasonic processing treatments (Fig. 3). Parameter estimates of the regression model are presented in Table 4, along with associated confidence limits.

Two aggregate cohorts (1 and 2; Table 4) of significantly ($p < 0.005$) different stability were detected within the studied soil, both composed of macroaggregates (>250 μm). Cohort 1 was represented within PSD tiers A (1000–2000 μm) and B (250–1000 μm), and cohort 2 was represented within tiers B and C (20–250 μm). The rate constant describing the breakdown rate of cohort 1 aggregates (0.004749 g J^{-1}) was significantly greater than that of cohort 2 (0.000325 g J^{-1}) at the 99.5% confidence level, indicating that cohort 2 aggregates have significantly greater ultrasonic stability than the relatively coarser cohort 1 aggregates. This difference in stability can be observed in Fig. 3. Tier A aggregates (composed of only cohort 1 aggregates) are seen to break down more rapidly than tier B aggregates, the latter including both cohort 1 and cohort 2 aggregates. Note that the two curves are qualitatively similar at low levels of applied energy (e.g. <150 J g^{-1}), where changes in the volume of each tier are due largely to comminution of the relatively unstable cohort 1 aggregates. At greater levels of applied energy (e.g. >330 J g^{-1}), very few cohort 1 aggregates remain intact, and change in the volume of tier B with increasing energy reflects only the (relatively slower) comminution of cohort 2 aggregates. North (1976) offered a similar interpretation regarding the observed comminution of >2 μm aggregates under ultrasound, suggesting that the early, rapid change in volume was due to breakdown of weak aggregates, and the "plateau" region of the curve at high energies reflected the breakdown of smaller, more-stable aggregates. Note also that these different rates of breakdown are reflected in the relative rates of accumulation of liberated particles in tiers D and E across corresponding ranges of applied energy. The proposed model identifies where such corresponding rates of change are occurring throughout ultrasonification in order to complete the dynamic mass mass-balance and determine the volume of particles of a given size liberated from aggregates of a particular stability. This enabled calculation of the PSD of particles liberated from cohort 1 to cohort 2 aggregates (presented below).

The volume (percent of total soil) of cohort 1 and cohort 2 aggregates was found to be similar at 24.8 and 29.7, respectively (Table 4).

Table 4
Model parameter estimates with 95% confidence limits

Cohort	Parameter	Estimate	95% CL (–)	95% CL (+)
1 (250–2000 μm)	a_1	0.004979	0.004431	0.005597
	b_{1A}	10.61	9.74	11.49
	b_{1B}	14.15	12.76	15.51
	b_{1C}	0	–	–
	b_{1D}	0	–	–
	$\int_0^{x_b} p_{1A}(x)dx$	1.00	–	–
	$\int_0^{x_c} p_{1AB}(x)dx$	0.66	0.60	0.72
	$\int_0^{x_d} p_{1ABC}(x)dx$	0.19	0.12	0.26
2 (20–1000 μm)	A_2	0.000325	0.000248	0.000405
	b_{2B}	12.05	10.47	13.78
	b_{2C}	17.62	16.04	19.70
	b_{2D}	0	–	–
	$\int_0^{x_c} p_{2B}(x)dx$	1.00	–	–
	$\int_0^{x_d} p_{2BC}(x)dx$	0.26	0.22	0.30
	δ_{0A}	0	–	–
	D_{0B}	28.76	27.85	29.66
	D_{0C}	48.37	47.45	49.28
	D_{0D}	10.25	9.34	11.16
	D_{0E}	1.92	1.04	2.79

The total volume of tier A, B, and C aggregates, irrespective of cohort affiliation, was 10.61, 26.2, and 17.62; indicating that approximately 68% of all detected soil aggregates were macroaggregates, of which roughly 30% were 1000–2000 μm. No aggregates were detected in tier D (2–20 μm). All volume changes of tier D were the result of liberation of either primary particles (or highly-stable microaggregates) from aggregates >20 μm. This is illustrated in Fig. 3, where accumulation of particles in tier D occurs continually throughout sonication, and at rates corresponding to rates of breakdown of cohort 1 and cohort 2 aggregates (this is also true for tier E). It should be noted, however, that complete disaggregation of >20 μm material was not quite achieved by the application of 5761 J g^{-1} of ultrasonic energy. It may be that with added energy a loss of volume would be observed in the 2–20 μm tier (indicating the presence of aggregates). Yet, in comparison to the maximum energies required to reach dispersion for the >2 μm fractions in Raine and So (1993) (approximately 1000 J g^{-1} at 8.9 W) and Field and Minasny (1999) (approximately 1800 J g^{-1} at 4.2 W) for studied Vertisols, the maximum applied energy in this study (5761 J g^{-1} at 14.2 W) is relatively large. This suggests that the observed 2–20 μm liberated particles are primary particles, or microaggregates unsusceptible to fragmentation by the power of applied ultrasound used in this study.

Interestingly, the volume of tier C (20–250 μm) exhibited an initial rise between $t=0$ and $t=90$ s of applied energy, followed by a steady decline during the remainder of the treatment (Table 3, Fig. 3). Modeling results indicate that the initial accumulation of 20–250 μm particles is due to the comminution of cohort 1 (>250 μm) aggregates, and the subsequent decline is due to the comminution of cohort 2 aggregates that liberated <20 μm particles. Similar behavior was observed by Oades and Waters (1991) for an Alfisol and a Mollisol subjected to a range of disruptive energy, where particles 20–250 μm were liberated from fragmented macroaggregates >250 μm, followed by breakdown of 20–250 μm particles to <20 μm particles. Levy et al. (1993) also observed a stepwise breakdown of aggregates under a range of applied ultrasonic energy. Field and Minasny (1999) and Field et al. (2006) modeled the accumulation and subsequent decline in the mass of PSD intervals between 2–20 μm and 2–100 μm for different soils subject to ultrasonic treatment, according to an analogue of a first-order consecutive kinetic reaction. These researchers interpreted the observed stepwise breakdown of aggregates to indicate the possible presence of a soil hierarchy, based upon the reasoning that soils with a hierarchy would be expected to exhibit a stepwise decline in breakdown rate as a soil is progressively agitated, reflecting the progressive fragmentation of larger aggregates and consequent liberation of smaller, hierarchically subordinate aggregates of greater stability.

This interpretation may indeed be accurate with respect to the behavior of tier C. However, the proposed model does not assume a hierarchical breakdown of aggregates, or that aggregates of differing stability are necessarily hierarchically related. Therefore, the model does not preclude the possibility that the observed accumulation and subsequent decline tier C volume is due to the release of primary particles from cohort 1 aggregates, offset by comminution of cohort 2 aggregates that existed discretely (i.e. not bound up in cohort 1 aggregates) before treatment. Indeed, two modeling results lend support to this latter interpretation. First, a considerably greater volume of cohort 2 particles (17.2% of soil total) was lost from tier C than was gained from cohort 1 (8.4%), suggesting that at least approximately half of tier C cohort 2 aggregates existed discretely prior to disturbance. Second, considering that the accumulation of primary particles (or highly-stable microaggregates) within tier D (2–20 μm) is partly due to the direct breakdown of cohort 1 aggregates to particles of this size, it seems reasonable to expect that some accumulation of primary/stable particles ≈ 20 μm or larger also occurred within tier C, and are responsible for at least part of the observed rise in tier C volume. Considering these two observations together, the alternative interpretation of tier C behavior appears plausible. Another possibility is that the observed is due to

Please cite this article as: Fristensky, A., Grismer, M.E., A simultaneous model for ultrasonic aggregate stability assessment, Catena (2008), doi:10.1016/j.catena.2008.04.013

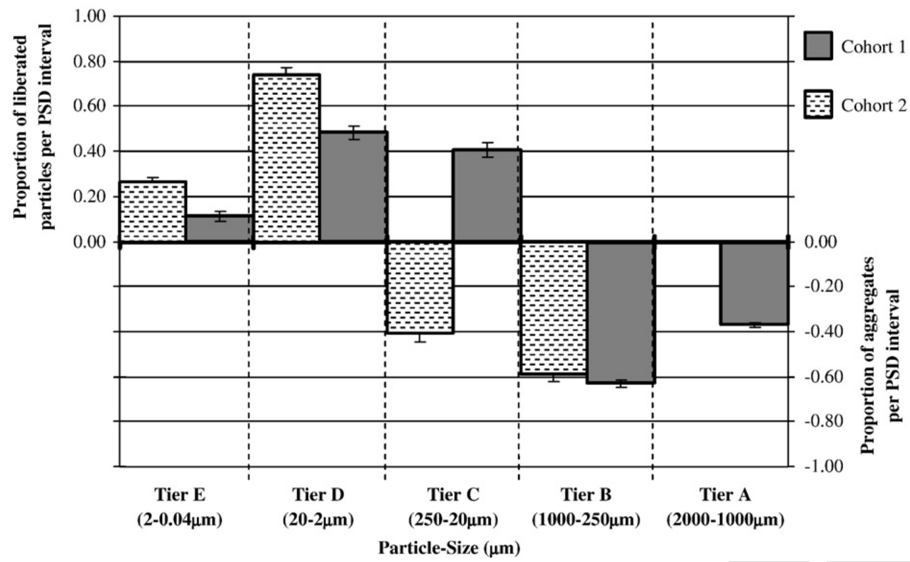

Fig. 4. PSD of cohort 1 and cohort 2 aggregates (below axis) and their fragments (above axis) ±95% confidence intervals.

accumulation of both primary particles and liberated aggregates. Without additional physical evidence, uncertainty exists regarding which scenario is accurate. Though not performed here, one way to gain a clearer picture of the relationship between the two observed cohorts would be to re-apply the model to a newly selected set of PSD partitions that provides greater resolution within the 20–250 μm fraction. Because an essentially continuous soil PSD was obtained from the laser-light technique, an unlimited number of such iterations could be conducted without the requirement of additional labwork. However, it is worth noting that owing to model independence from assumptions regarding soil hierarchy, calculations of the volume, stability, and PSD of liberated particles of cohort 1 or cohort 2 aggregates do not depend upon identifying whether these aggregates are hierarchically related.

Significant differences ($p \leq 0.05$) were observed in the PSD of particles liberated from cohort 1 and cohort 2 aggregates. Fig. 4 is analogous to the conceptual model displayed in Fig. 1, illustrating the size distribution of cohort 1 and cohort 2 aggregates (below the axis), as well as the distribution of their respective liberated particles (above the axis).

The distributions in Fig. 4 are discrete blocks, rather than continuous as in Fig. 1, representing the average values of the $p_i(x)$ and $q_i(x)$ within the selected PSD tiers. The PSD of particles liberated from cohort 1 is coarser than that of cohort 2; i.e. particles liberated from cohort 2 aggregates are comprised of a significantly greater proportion of clay-sized (<2 μm) and fine silt-sized (2–20 μm) particles than cohort 1 aggregates. Only cohort 1 was found to be comprised of particles 20–250 μm in size. These results suggest that with a mild agitation applied to the soil (i.e. disrupting the relatively weak cohort 1 aggregates, but not necessarily the more-stable cohort 2 aggregates), aggregate comminution would result principally in the release of roughly equal proportions 2–20 μm and 20–250 μm particles, with a relatively small fraction of clay released. In contrast, a relatively more energetic disruption of the soil may result in the release of much larger amounts of clay and fine silt, due to comminution of the relatively stable cohort 2 aggregates.

3.3. Model comparison

In previous studies (e.g., Fuller and Goh, 1992; Levy et al., 1993; Raine and So, 1993), exponential functions involving only a single rate constant were used to model the breakdown of aggregates within selected PSD intervals. Such models obtain a single constant describing the rate of breakdown of all aggregates with the selected interval. However, aggregates of differing stability may exist within a given particle-size interval, breaking down at different rates. In the current instance, allowing for the presence of aggregates of distinctly different stability (i.e. allowing more than one rate constant to describe aggregate breakdown) obtains a significantly ($p \leq 0.0001$) better fit than modeling these tiers according the simple decay function used in the cited studies. Table 5 presents the results of F-test comparisons between the proposed model ("full model") and an

Table 5
F-test model comparisons (single exponential vs. proposed) for tiers B, D, E

Tier	Model	Exponential (reduced)	Proposed (full)							Conclude[a]
	Parameter	F_0	A_0	k	D_0	[b]b^*_1	[b]b^*_2	a_1	a_2	
B	Estimate	7.01	20.13	0.0021	28.76	14.15	12.05	0.004979	0.000325	Reject H_0
	MSE	5.52			2.11					
	F-value	27.62								
	Critical F[c]	12.58								
D	Estimate	13.77	26.09	0.000971	10.25	13.12	21.96	0.004979	0.000325	Reject H_0
	MSE	4.32			1.01					
	F-value	54.96								
	Critical F[c]	12.58								
E	Estimate	2.92	8.52	0.000676	1.92	2.72	7.71	0.004979	0.000325	Reject H_0
	MSE	0.26			0.08					
	F-value	35.15								
	Critical F[c]	12.58								

[a] Null (H_0) and alternative (H_a) hypotheses explained in text.
[b] The b^*_i are the total volume contributed to or lost from the jth tier due to the ith cohort.
[c] The critical F-value for $\alpha = 0.0001$.

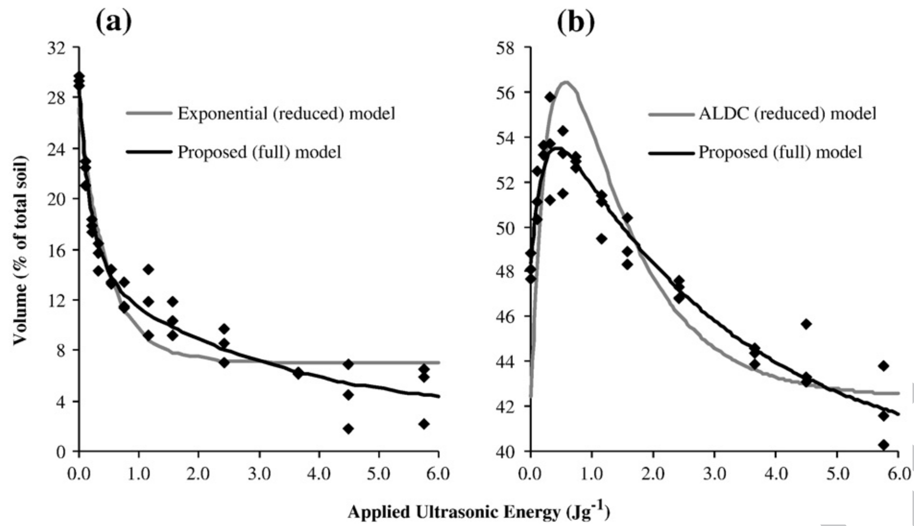

Fig. 5. Comparison of the regression fit of the proposed (full) model vs. alternative (reduced) models. (a) The proposed model vs. simple exponential decay for tier B (250–1000 μm). (b) The proposed model vs. the ALDC (Field and Minasny (1999) for tier C (20–250 μm).

exponential decay (or approach) function ("reduced model"). The full model was found to be statistically more appropriate than the reduced model for PSD tiers B, D, and E. Fig. 5(a) illustrates the improved fit of the full model relative to the reduced model. These results support the finding of the proposed model that tier B aggregates consisted of two groups of aggregates with distinctly different stability (cohorts 1 and 2), and that volume changes in tiers D and E ultrasonification are due to the breakdown of both cohort 1 and cohort 2 aggregates. Notably, for all three tiers (B, D, E), the value of the estimated rate constant for the reduced model was between those of the two rate constants obtained for the full model (Table 5). Also, the reduced model estimates of the volume of aggregates or accumulated particles in each tier were always smaller than those obtained by the full model.

The results of the proposed model for tier C were compared with those obtained by fitting the ALDC (Field and Minasny, 1999) to this dataset. It should be noted that the ALDC assumes that the modeled aggregates comminute in a stepwise fashion according a particular consecutive reaction pathway, with the steps corresponding to the selected PSD intervals (in this case, <2 μm, 20–250 μm, and >250 μm) (Field and Minasny, 1999; Field et al., 2006). Consequently, because the PSD range of tier C was selected irrespective of expectations regarding the structure or hierarchy of the studied soil aggregates, the ALDC may not be appropriate in this instance, and therefore comparisons between the two models may not be valid. However, considering that no alternative model except the ALDC currently exists for analysis of the type of behavior displayed in tier C, comparison of the two models seems justified. Results of an F-test comparison between the proposed model and the ALDC are presented in Table 6; indicating that the full model is statistically ($p<0.0001$) more appropriate than the ALDC for this dataset. Notably, the ALDC predicts a significantly ($p<0.005$) larger rate constant ($0.00063\ \mathrm{g\ J^{-1}} \leq k_2 \leq 0.00127\ \mathrm{g\ J^{-1}}$) describing the breakdown of 20–250 μm aggregates compared to that of the full model ($0.00022 \leq a_2 \leq 0.00044$), as illustrated in Fig. 5(b). Hence, in this instance, the ALDC predicts 20–250 μm aggregates to be less stable than predicted by the proposed model.

In addition to the potential enhancements in detecting, resolving, and modeling aggregates of differing stability afforded by the proposed model, simultaneous analysis of multiple particle-size intervals spanning both microaggregate and macroaggregate fractions may also aid interpretation of soil dispersion data. For instance, fitting an exponential approach model individually to the <20 μm and <2 μm fractions of the studied soil obtains estimated rate constants of $a_{20\ \mu m}=0.000885$ and $a_{2\ \mu m}=0.000676$, respectively. Considering only the >20, <20, and <2 μm PSD intervals, the relationship $a_{20\ \mu m}>a_{2\ \mu m}$ might suggest the existence of 2–20 μm microaggregates according to the interpretation offered by Field and Minasny (1999). However, results of the proposed model indicate that the observed differences in the rate of change of the <20 μm and <2 μm fractions are due to different rates of breakdown of cohort 1 and cohort 2 macroaggregates, which directly liberate different proportions of 2–20 μm and <2 μm particles. Yet, without simultaneously investigating several discrete PSD fractions in

Table 6
F-test comparison for the ALDC and proposed models for tier C

Model	Parameter	Estimate	MSE	F-value (critical F[a])	Conclude[b]
ALDC (reduced)	C_2	42.40	7.84	52.59 (10.12)	Reject H_0
	A_0	32.73			
	k_1	0.0031057			
	k_2	0.0008992			
Proposed (full)	D_0	48.37	1.34		
	b_{1A}	10.61			
	b_{1B}	14.15			
	$\int_0^{x_c} p_{1AB}(x)dx$	0.66			
	b_{2C}	17.62			
	a_1	0.004979			
	a_2	0.000325			

[a]The critical F-value for $\alpha=0.0001$.
[b]Null (H_0) and alternative (H_a) hypotheses explained in text.
The critical F-value for $\alpha=0.0001$.

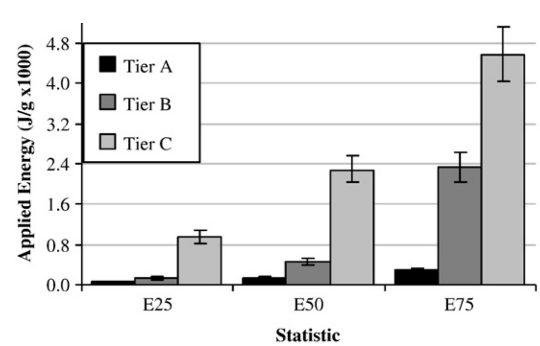

Fig. 6. The ultrasonic energy required to disrupt 25% (E_{25}), 50% (E_{50}), and 75% (E_{75}) of all aggregates for tiers A (1000–2000 μm), B (250–1000 μm), and C (20–250 μm).

Please cite this article as: Fristensky, A., Grismer, M.E., A simultaneous model for ultrasonic aggregate stability assessment, Catena (2008), doi:10.1016/j.catena.2008.04.013

both the microaggregate and macroaggregate fractions, we might have alternatively concluded that the studied soil possesses microaggregates of size 2–20 μm that breakdown at rate $a_{2\ \mu m}$.

3.4. Stability indices E_{25}, E_{50} and E_{75}

Throughout the previous discussion, the breakdown and stability of aggregates throughout the soil has been described in terms of the behavior of aggregate cohorts. However, as the number, particle-size domain, stability, and interrelationships of aggregate cohorts will vary between different soils, characterizing aggregate stability in terms of cohort behavior is not amenable to comparative analyses. Quantifying aggregate stability according to the behavior of discrete PSD partitions (e.g. 250–1000 μm) facilitates comparison between different soils. Similar to Fuller and Goh (1992) who calculated the ultrasonic energy required to disrupt 50% of aggregates (E_{50}), based upon results of the proposed model we calculated the level of ultrasonic energy required to observe a 25%, 50%, and 75% reduction in the total volume of all aggregates within a particular PSD tier. These three energy levels E_{25}, E_{50}, and E_{75}, respectively. Estimates of these levels for tiers A, B, and C are illustrated in Fig. 6. The E_{50} of all tier A aggregates was 146 J g^{-1}. This level of energy was significantly ($p < 0.005$) less than E_{50} for tier B, at 451 J g^{-1}; of which was also significantly ($p < 0.005$) less than E_{50} for tier C (2279 J g^{-1}). Identical rankings were obtained for these three tiers with respect to the E_{25} and E_{75} statistics at the $\alpha = 0.05$ level.

As above, these results indicate that the stability of aggregates declines significantly with increasing size. The 1000–2000 μm aggregates are the least-stable aggregates observed in this soil, showing relatively rapid disruption with applied energy. Considering that the aggregate cohort represented within this particle-size interval was found to directly liberate 60% of its volume as <20 μm particles, and approximately 10% as clay (2 μm), disruption of these aggregates by rainfall impact may lead to reduced infiltration and increased runoff due to loss of high conductivity >100 μm pores (Oades, 1984) and formation of a structural crust (Moss, 1991). The increased transport capacity of overland flow due to increased runoff volume, together with an increase in fine particles with low settling rates detached from disrupted aggregates, may enhance erosion potential (Owoputi and Stolte, 1995; Green and Hairsine, 2004). However, the degree to which the ultrasonic stability indices presented above relate to soil erodibility has not been ascertained here. Further research relating these indices to, for example, rainfall simulation variables (similar to Legout et al., 2005 and Le Bissonnais et al., 2007) will help assess the facility of the presented method in predicting soil susceptibility to erosion.

4. Summary and conclusions

The model and experimental approach described above provides a method for analyzing the comminution and ultrasonic stability of aggregates across several PSD partitions spanning both the macroaggregate (<250 μm) and macroaggregate (>250 μm) fractions. Independence of the proposed model from assumptions regarding the constituent particle-size or hierarchical structure of aggregates confers universal applicability, and greater flexibility relative to alternative methods. Expanding the model to the simultaneous analysis of several particle-size intervals enables researchers to investigate aggregate comminution dynamics throughout any set of PSDs partitions selected according to individual research interests. For a studied Dystroxerept subject a range of ultrasonic energy, the proposed model statistically outperformed alternative models in accounting for observed changes in the total volume of 4 out of 5 selected microaggregate and macroaggregate fractions, and offered greater resolution of aggregate comminution dynamics and the PSD of particles liberated from groups of aggregates exhibiting similar stability. Possible evidence of a hierarchical relationship was detected between two group aggregates exhibiting distinctly different stability; however, additional evidence (e.g. varying or increasing the number of selected PSD partitions) was needed to rule out alternative explanations of the observed behavior.

Similar to existing methods, the proposed model assumes that breakdown of a quantity of aggregates follows exponential decay under ultrasonification. While this model has obtained a good regression fit of experimental data both here and in previous ultrasonic studies, it may not be appropriate for all soils or at all particle-size scales. In addition to this fundamental assumption, potential limitations of the proposed model include: (1) underestimation of the mass or volume of aggregates of a particular size, due to the inability to detect a redistribution of particle-sizes within a given PSD interval; (2) inability to detect whether particles are being accumulated and lost from a PSD interval at an identical rate, possibly leading to inaccurate identification of the size (though not of the stability) of source aggregates of liberated particles; and (3) possible variations in modeling results due to (1) and (2) as the number and particle-size domain of the selected PSD intervals changes. Increasing the number of selected PSD intervals will increase modeling resolution and mitigate errors arising from (1) and (2); but the extent to which this is possible is limited by the rapid increase in model complexity with added PSD partitions; by the resolution of the PSD measurement technique; and by soil variability.

The laser-light diffraction technique for particle-size analysis was critical to this analysis, providing precise, non-disruptive measurements of changes in volume of both microaggregate and macroaggregate fractions; and demonstrating that ultrasonic methods can be usefully employed for targeted stability assessment of macroaggregate subgroups. Analysis of different macroaggregate subgroups offered enhanced resolution of aggregate comminution dynamics, and helped explain the variation observed in finer PSD intervals throughout the ultrasonic treatment. Altogether, the model and experimental approach presented here offered insight into the stability, constituent PSD, and comminution dynamics of soil aggregates. Both the flexibility of the proposed model and extension of ultrasonic stability assessment to simultaneous analysis of both microaggregate and macroaggregate subgroups can facilitate broader application of ultrasonic methods for soil processes related research.

References

Alvord, W.G., Rossio, J.L., 1993. Determining confidence limits for drug potency in immunoassay. J. Immunol. Methods 157, 155–163.

Amezketa, E., 1999. Soil aggregate stability: a review. J. Sustain. Agric. 14 (2–3), 83–151.

Arras, K.O., 1998. An introduction to error propagation. Technical Report No. EPFL-ASL-TR-98-01 R3. Autonomous Systems Lab, Institute of Robotic Systems. Swiss Federal Institute of Technology Lausanne (EPFL).

Beuselinck, L., Govers, G., Poeson, J., Degraer, G., Froyen, L., 1998. Grain-size analysis by laser diffractometry: comparison with the sieve-pipette method. Catena 32, 193–208.

Braunack, M.V., Hewitt, J.S., Dexter, A.R., 1979. Brittle fracture of soil aggregates and the compaction of aggregate beds. J. Soil Sci. 30, 653–667.

Dexter, A.R., 1988. Advances in characterization of soil structure. Soil Tillage Res. 11.

Edwards, A.P., Bremner, J.M., 1967. Microaggregates in soil. J. Soil Sci. 18, 64–73.

Eshel, G., Levy, G.J., Mingelgrin, U., Singer, M.J., 2004. Critical evaluation of the use of laser diffraction for particle-size distribution analysis. Soil Sci. Soc. Am. J. 68 (3), 736–743.

Field, D.J., Minasny, B., 1999. A description of aggregate liberation and dispersion in A horizons of Australian Vertisols by ultrasonic agitation. Geoderma 91 (1–2), 11–26.

Field, D.J., Minasny, B., Gaggin, M., 2006. Modelling aggregate liberation and dispersion of three soil types exposed to ultrasonic agitation. Aust. J. Soil Res. 44 (5), 497–502.

Fuller, L.G., Goh, T.B., 1992. Stability-energy relationships and their application to aggregation studies. Can. J. Soil Sci. 72 (4), 453–466.

Gee, G.W., Bauder, J.W., 1986. Particle-size analysis. In: Klute, A. (Ed.), Methods of Soil Analysis, Part 1, Physical and Mineralogical Methods. ASA, Madison, WI, pp. 383–411.

Green, R.S.B., Hairsine, P.B., 2004. Elementary processes of soil–water interaction and thresholds in soil surface dynamics: a review. Earth Surf. Processes Landf. 29, 1077–1091.

Imeson, A.C., Vis, M., 1984. Assessing soil aggregate stability by water-drop impact and ultrasonic dispersion. Geoderma 34 (3–4), 185–200.

Integrated Environmental Restoration Services (IERS), 2007. Monitoring and Assessment of Erosion Control Treatments in and around the Lake Tahoe Basin. Integrated Environmental Restoration Services, Tahoe City, CA.

Kragten, J., 1994. Calculating standard deviations and confidence-intervals with a universally applicable spreadsheet technique. Analyst 119 (10), 2161–2165.

Kutner, M.H., Nachtsheim, C.J., Neter, J., Li, W., 2005. Applied Linear Statistical Models. McGraw-Hill Irwin, New York, NY. 1396 pp.

Please cite this article as: Fristensky, A., Grismer, M.E., A simultaneous model for ultrasonic aggregate stability assessment, Catena (2008), doi:10.1016/j.catena.2008.04.013

Levy, G.J., Agassi, M., Smith, H.J.C., Stern, R., 1993. Microaggregate stability of kaolinitic and illitic soils determined by ultrasonic energy. Soil Sci. Soc. Am. J. 57 (3), 803–808.

Moss, A.J., 1991. Rain-impact soil crust. 1. Formation on a granite derived soil. Aust. J. Soil Res. 29, 271–289.

North, P.F., 1976. Towards an absolute measurement of soil structural stability using ultrasound. J. Soil Sci. 27, 451–459.

North, P.F., 1979. Assessment of the ultrasonic method of determining soil structural stability in relation to soil management properties. J. Soil Sci. 30, 463–472.

Oades, J.M., 1984. Soil organic-matter and structural stability — mechanisms and implications for management. Plant Soil 76 (1–3), 319–337.

Q10 Oades, J.M., Water, A.G., 1991. Aggregate hierarchy in soil. Aust. J. Soil Res. 29, 815–828.

Owoputi, L.O., Stolte, W.J., 1995. Soil detachment in the physically-based soil-erosion process — a review. Trans. ASAE 38 (4), 1099–1110.

Raine, S.R., So, H.B., 1993. An energy-based parameter for the assessment of aggregate bond-energy. J. Soil Sci. 44 (2), 249–259.

Raine, S.R., So, H.B., 1994. Ultrasonic dispersion of soil in water — the effect of suspension properties on energy-dissipation and soil dispersion. Aust. J. Soil Res. 32 (6), 1157–1174.

Raine, S.R., So, H.B., 1997. An investigation of the relationships between dispersion, power, and mechanical energy using the end-over-end shaking and ultrasonic methods of aggregate stability assessment. Aust. J. Soil Res. 35 (1), 41–53.

Roscoe, R., Buurman, P., Velthorst, E.J., 2000. Disruption of soil aggregates by varied amounts of ultrasonic energy in fractionation of organic matter of a clay Latosol: carbon, nitrogen and delta C-13 distribution in particle-size fractions. Eur. J. Soil Sci. 51 (3), 445–454.

Soil Survey Staff, N.R.C.S., United States Department of Agriculture, 2007. Official Soil Series Descriptions. [Online WWW]. Available URL: "http://soils.usda.gov/technical/classification/osd/index.html" [Accessed 22 July 2007].

Tippkotter, R., 1994. The effect of ultrasound on the stability of mesoaggregates (60–2,000 mu). Z. PflanzenernaÉhr. Bodenkd. 157 (2), 99–104.

Tisdall, J.M., Oades, J.M., 1979. Stabilization of soil aggregates by the root systems of ryegrass. Aust. J. Soil Res. 17 (3), 429–441.

Tisdall, J.M., Oades, J.M., 1982. Organic-matter and water-stable aggregates in soils. J. Soil Sci. 33 (2), 141–163.

Utomo, W.H., Dexter, A.R., 1981. Soil friability. J. Soil Sci. 32 (2), 203–213.

Please cite this article as: Fristensky, A., Grismer, M.E., A simultaneous model for ultrasonic aggregate stability assessment, Catena (2008), doi:10.1016/j.catena.2008.04.013